

# NLO corrections to electroweak and QCD production of $W^+W^+$ plus two jets in the POWHEG BOX

---

**Barbara Jäger**

*Institut für Physik (THEP), Johannes-Gutenberg-Universität, 55099 Mainz, Germany*  
*E-mail: jaegerba@uni-mainz.de*

**Giulia Zanderighi**

*Rudolf Peierls Centre for Theoretical Physics, 1 Keble Road, University of Oxford, UK*  
*E-mail: g.zanderighi1@physics.ox.ac.uk*

**ABSTRACT:** We present the matching of the next-to-leading order QCD calculation for  $W^+W^+jj$  production via vector-boson fusion in hadronic collisions to parton-shower Monte-Carlo programs according to the POWHEG method. Our implementation complements existing code for QCD-induced  $W^+W^+jj$  production in the POWHEG BOX package, thereby providing a platform for the complete Standard Model production of  $W^+W^+jj$  events via QCD and electroweak interactions. The impact of parton-shower effects is discussed for various distributions and found to be small in most cases. However, few observables, that are relevant for analyses using a central jet veto, are modified significantly when they are interfaced to a parton shower program.

**KEYWORDS:** POWHEG, NLO, QCD, SMC.

---

## Contents

<b>1. Introduction</b>	<b>1</b>
<b>2. Technical details</b>	<b>3</b>
2.1 Next-to-leading order QCD corrections to VBF $W^+W^+jj$ production	3
2.2 The POWHEG BOX implementation	4
2.3 Validation and checks	6
<b>3. Phenomenological results</b>	<b>6</b>
<b>4. Conclusion</b>	<b>13</b>

---

## 1. Introduction

With the start-up of the CERN Large Hadron Collider (LHC) the production of multi-particle final states at high energies has become feasible. The analysis and interpretation of these measurements requires accurate predictions for processes of high multiplicity. The past years have seen an exceptional progress in the development of new techniques suitable for the calculation of next-to-leading order (NLO) QCD corrections to multi-particle production processes at hadron colliders (see [1] for a pedagogical review on these techniques). These advances resulted in a large number of NLO calculations of multi-particle production processes in the last two years [2–19]. While NLO-QCD predictions are essential to reduce the theoretical uncertainties associated with the hard scattering process, a description of the additional hadronic activity in realistic LHC events relies on parton-shower generators such as HERWIG [20, 21] or PYTHIA [22]. The perturbative accuracy of these programs is however limited, formally, to leading logarithmic accuracy. Combining the benefits of an NLO-QCD calculation with those of a parton-shower program yields the most realistic, yet accurate, results for scattering processes at hadron colliders feasible to date.

Currently, two frameworks are available to combine NLO-QCD calculations with parton shower programs: MC@NLO [23] and POWHEG [24, 25]. aMC@NLO is a recent further development of the former approach that aims at a fully automated event generation at NLO in QCD [26]. A first phenomenological application of aMC@NLO, has been the implementation of a (pseudo)-scalar Higgs in association with a  $t\bar{t}$  pair [27]. The POWHEG method has been utilized by several groups, e.g., in the context of HERWIG++ [28, 29], or Sherpa [30, 31]. Recently, the method has been used also for  $t\bar{t}$  pair production in association with one jet [32] and in association with a Higgs boson [33] in the HELAC framework.

As a tool for merging NLO-QCD calculations for arbitrary processes with any parton shower program in the POWHEG approach, the so-called POWHEG BOX [34] was developed

one year ago. It requires few process-specific building blocks: the Born and real-emission squared amplitudes, the finite parts of the virtual squared amplitude, color- and spin-correlated Born amplitudes, the Born phase-space and the flavor structure of all contributing Born and real subprocesses. All these elements are essentially readily available once a NLO calculation for a given process has been performed. Thus the implementation in the `POWHEG BOX` of a new process that is known at NLO requires in general only little effort. All further ingredients for the merging procedure and the subtraction of singularities are provided by the `POWHEG BOX`. Using this method, a large number of NLO-QCD calculations has been matched to parton-shower programs recently and is currently in the public repository of the `POWHEG BOX`: heavy flavor pair production [35], Higgs production via gluon fusion [36] and via vector boson fusion (VBF) [37], vector boson [38] and vector boson plus jet production [39], single top production [40, 41], jet pair production [42],  $Wb\bar{b}$  production [43], vector boson pair production [44], and QCD-induced  $W^+W^+jj$  production [45].

This last process,  $W^+W^+jj$  production, exhibits several interesting phenomenological features. Due to its exotic signature with two same-sign leptons, missing energy, and two jets it comprises an important background to double parton scattering [46, 47]. Understanding this class of processes is of paramount importance for a realistic description of the collider environment in which hard scattering reactions take place. Moreover,  $W^+W^+jj$  production constitutes a background for new physics scenarios involving same-sign leptons, such as R-parity violating SUSY models [48] or doubly charged Higgs production [49].

In the Standard Model (SM) there are two direct hard production mechanisms that give rise to the same  $W^+W^+jj$  final state: the QCD production, which proceeds via gluon-mediated (anti-)quark scattering processes with the two  $W^+$  bosons being radiated each off one of the fermion lines (this is the process already included in the `POWHEG BOX`), and electroweak (EW) production, where a color neutral vector boson connects the two quark lines and the  $W^+$  bosons are emitted either from the quarks or from the exchanged vector boson.

At leading order, due to color conservation, the QCD and EW production modes do not interfere and can thus be discussed separately. Because of the hierarchy between the QCD and the EW coupling, one would expect the QCD-induced  $W^+W^+jj$  production,  $\mathcal{O}(\alpha_s^2\alpha^4)$ , to fully dominate over the EW production mode,  $\mathcal{O}(\alpha^6)$ . Explicit calculations revealed, however, that the inclusive QCD production cross section of  $W^+W^+jj$  final states is only roughly twice as large as the corresponding EW one [46]. This means that an accurate description of the inclusive SM production of  $W^+W^+jj$  must take both production modes into account. Furthermore, when typical VBF cuts are imposed on the final state, the QCD-production cross-section drops drastically and the SM cross-section is fully dominated by the EW production mode.

NLO-QCD predictions for EW  $W^+W^+jj$  production have been available for some time [10]. More recently, QCD corrections have been provided also for the QCD production mode [14], and elements of this latter calculation have already been implemented in the `POWHEG BOX`. To allow for a complete SM description of the  $W^+W^+jj$  final state at NLO-QCD accuracy with parton-shower effects, we implement the EW production mode in the same framework too. The calculation of Ref. [10] includes non-resonant diagrams, takes

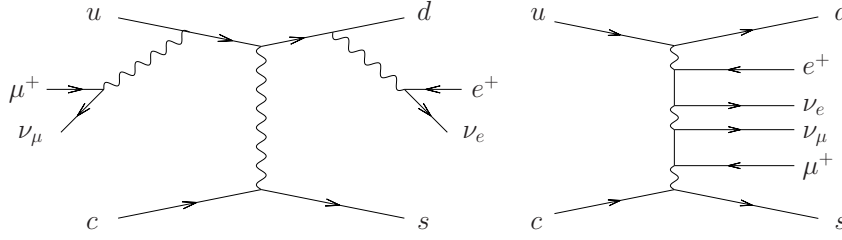


**Figure 1:** Resonant (a) and non-resonant (b) sample diagrams for the partonic subprocess  $u(1)c(2) \rightarrow e^+(3)\nu_e(4)\mu^+(5)\nu_\mu(6)d(7)s(8)$  at leading order.

off-shell effects and spin-correlations of the leptonic  $W$  decays fully into account.

For definiteness, results presented in this paper are based on the decays of the  $W$ -bosons to  $e^+\nu_e\mu^+\nu_\mu$ . Neglecting interference effects in the case of identical leptons, the cross-section for the  $W$ -bosons to decay to any lepton ( $e^+, \mu^+, \tau^+$ ) can be obtained by multiplying our results by nine over two.

We also note that, while we discuss here  $W^+W^+$  production, which is dominant at the LHC, it is also trivial to obtain results for  $W^-W^-$ . Indeed, using charge conjugation and parity,  $pp \rightarrow W^-W^-jj$  is almost equivalent to  $\bar{p}\bar{p} \rightarrow W^+W^+jj$ , modulo reversing the momentum directions for parity-odd distributions.

The outline of this paper is as follows: In Sec. 2 we describe the technical details of the NLO-QCD calculation for VBF  $W^+W^+jj$  production, its implementation in the POWHEG BOX, and the checks we have performed. In Sec. 3 we discuss phenomenological results for several kinematic distributions with particular emphasis on the impact parton-shower effects have on the NLO-QCD predictions. Cross sections and distributions for the VBF production mode are compared to the same observables of the QCD production mode. We conclude in Sec. 4.

## 2. Technical details

### 2.1 Next-to-leading order QCD corrections to VBF $W^+W^+jj$ production

The partonic scattering amplitudes which are needed for the calculation of cross sections and distributions at NLO-QCD accuracy and their combination with parton-shower programs via the POWHEG BOX are extracted from previous work on VBF  $W^+W^+jj$  production in the `vbfnlo` framework [50]. Here, we summarize only the elements of the calculation which are relevant for its implementation in the POWHEG BOX. For technical details on the NLO calculation, we refer the interested reader to Ref. [10]

At order  $\alpha^6$ , EW production mainly proceeds via the scattering of two (anti-)quarks by  $t$ -channel exchange of a weak gauge boson with subsequent emission of two  $W^+$  bosons, which in turn decay leptonically. Non-resonant diagrams where leptons are produced via weak interactions in the  $t$ -channel also contribute. Sample diagrams for both of these topologies are depicted in Fig. 1 for the representative subprocess  $uc \rightarrow e^+\nu_e\mu^+\nu_\mu ds$ . In principle, also quark-antiquark annihilation processes with weak-boson exchange in the  $s$ -channel and subsequent decay into a pair of jets have to be considered. However, they

are strongly suppressed in the phase space regions where the VBF process can be observed experimentally [51], and thus disregarded. For subprocesses with identical flavor combinations, such as  $uu \rightarrow e^+\nu_e\mu^+\nu_\mu dd$ , in addition to the  $t$ -channel contributions discussed above also  $u$ -channel diagrams and their interference with the  $t$ -channel graphs arise. While we do take into account both  $t$ - and  $u$ -channel contributions, we do not consider their interference cross section, which is kinematically strongly suppressed [51]. For brevity, we will refer to  $pp \rightarrow e^+\nu_e\mu^+\nu_\mu jj$  as “VBF  $W^+W^+jj$ ” production in the following, even though the electroweak production process includes non-resonant diagrams that do not stem from a  $W^+$  decay (see e.g. Fig. 1b).

The NLO-QCD corrections to VBF  $W^+W^+jj$  production consist of two types of contributions: one-loop corrections to the leading order (LO) diagrams and real-emission contributions with an extra parton in the final state. The real-emission amplitudes are obtained by attaching a gluon to the tree-level diagrams discussed above. Crossing-related processes with a gluon in the initial state also contribute. The virtual corrections comprise the interference of one-loop diagrams with the tree-level amplitude. Within our approximations, only selfenergy-, triangle-, box-, and pentagon-corrections to either fermion line have to be considered. Diagrams with a gluon being exchanged between upper and lower quark lines vanish when interfered with the Born amplitude, due to color conservation. The finite parts of the virtual corrections are evaluated numerically by means of a Passarino-Veltman tensor reduction. In order to avoid numerical instabilities in the evaluation of the five-point tensor integrals, we resort to the Denner-Dittmaier reduction scheme of Refs. [52,53]. The numerical stability of our implementation is monitored by checking Ward identities at every phase space point. While in the NLO-QCD calculation of Ref. [10] infrared singularities arising in both real emission and virtual contributions were handled by the dipole subtraction approach of Catani and Seymour [54], the POWHEG BOX internally takes care of these divergences via the Frixione-Kunszt-Signer subtraction approach [55].

As in the NLO calculation in [10] we neglect quark masses, and entirely disregard contributions from external  $b$  and  $t$  quarks. We also assume a diagonal CKM matrix.

## 2.2 The POWHEG BOX implementation

We have implemented our NLO-QCD calculation for  $pp \rightarrow e^+\nu_e\mu^+\nu_\mu jj$  via VBF in the POWHEG BOX by providing the following ingredients:

- the list of all independent flavor structures of the Born process,
- the list of all independent flavor structures of the real emission process,
- the Born phase space,
- the Born squared amplitude,
- the color-correlated and the spin-correlated Born squared amplitude,
- the real-emission squared amplitudes for all contributing sub-processes,
- the finite part of the virtual amplitudes interfered with the Born,

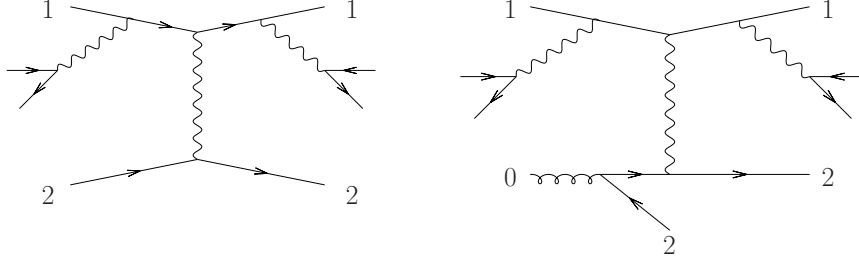


**Figure 2:** Tag assignment for representative contributions to the Born process  $uc \rightarrow e^+\nu_e\mu^+\nu_\mu ds$  and the gluon-initiated real-radiation process  $ug \rightarrow e^+\nu_e\mu^+\nu_\mu ds\bar{c}$ . Zero tags for the leptons are not explicitly indicated in the diagrams.

- the color structure of the Born process in the limit of a large number of colors.

In order to comply with the ordering scheme required by the **POWHEG BOX**, we assign identifiers to the partons and leptons of each tree-level subprocess in the following way:

- 1. incoming parton with positive rapidity,
- 2. incoming parton with negative rapidity,
- 3. – 6. final state charged leptons and neutrinos,
- 7. – 8. final-state partons.

For example, the particles involved in the representative subprocess of Fig. 1 are ordered in the following way:  $u(1)c(2) \rightarrow e^+(3)\nu_e(4)\mu^+(5)\nu_\mu(6)d(7)s(8)$ , where the numbers in parentheses denote the identifiers. In the real-emission configurations, the extra final-state parton is referred to as ninth particle.

Spin-correlated Born amplitudes generally arise only if external gluons emerge at tree-level, which is not the case in VBF processes. Due to the simple color structure of the process, the only non-vanishing color-correlated amplitudes  $\mathcal{B}_{ij}$  for a pair of partons  $ij$  are just multiples of the Born amplitude  $\mathcal{B}$  itself,

$$\mathcal{B}_{17} = \mathcal{B}_{28} = C_F \mathcal{B}, \quad (2.1)$$

where  $C_F = 4/3$ . The assignment of color flow is straightforward and unambiguous: it follows directly the propagation of the QCD partons.

In VBF processes, there is no interference between radiation off the upper and lower fermion lines because of the color-singlet nature of the weak-boson exchange in the  $t$ -channel. In order to pass this extra information to the **POWHEG BOX** while searching for singular regions, a tag is assigned to each quark line, as explained in some detail in Ref. [37] for the related process of Higgs production via VBF. Particles that do not need to be tagged are assigned a tag equal to zero, as illustrated in Fig. 2. The tags are taken into account by the **POWHEG BOX** when singular regions for the generation of radiation are identified, but have no further consequences for the flavor arrangements. The total LO cross section for  $pp \rightarrow W^+W^+jj$  is finite. We therefore apply a phase space generator that covers all

phase space. Generation cuts are not needed. In the code,  $W$ -bosons can be generated both on-shell or off-shell with a Breit-Wigner distribution, according to the setting in the `powheg.input` file, see the `VBF_Wp_Wp` manual for details.

We note that the implementation of the VBF  $W^+W^+jj$  process in the `POWHEG BOX` was straightforward. Following the procedure of Ref. [37] for the tagging of quark lines as described above and exploiting the technical developments of Ref. [45] for the efficient treatment of a multi-leg process, we were able to obtain a stable code without any further systematic refinements.

### 2.3 Validation and checks

While the `POWHEG BOX` offers a flexible environment for hadronic scattering processes at NLO-QCD accuracy, the actual implementation of the required building blocks requires care by the individual user and has to be validated thoroughly.

A valuable check for the correct implementation of the tree-level and real-emission contributions of individual subprocesses as well as their flavor sum is provided by the `POWHEG BOX` itself. It computes the soft and collinear limits of the real-emission cross section internally, using only the user-supplemented Born amplitudes. The `POWHEG BOX` then checks automatically, whether these approach the full real-emission contributions in all soft and collinear regions. The result of this comparison is written to a user-readable file at the beginning of each production run.

The `POWHEG BOX` does not only offer a framework for interfacing NLO-QCD calculations to parton-shower programs, but can also be used in a stand-alone mode for the calculation of cross sections and distributions at LO and NLO-QCD accuracy. Using this option, we have generated a multitude of distributions both at LO and NLO QCD, and compared the results with those we obtained with the parton-level Monte-Carlo program of Ref. [10]. We found full agreement for all observables.

## 3. Phenomenological results

The implementation of VBF  $W^+W^+jj$  in the `POWHEG BOX` has been made publicly available. The interested reader can thus generate any required distributions with all settings adapted to her needs. The default setup of the code is identical to the QCD  $W^+W^+jj$  production process in the `POWHEG BOX`, which has already been discussed in Ref. [45]. This should facilitate a comparison of the two production modes in a common environment. Here, we discuss only a few selected results for representative input parameters and selection cuts. We restrict ourselves to the  $e^+\nu_e\mu^+\nu_\mu jj$  final state with two charged leptons of different type and their associated neutrinos. The full cross section summed over electrons and muons can be obtained thereof by multiplying with a factor of two in the approximation that interference effects for same-type lepton contributions are neglected.

We consider proton-proton collisions at a center-of-mass energy of  $\sqrt{s} = 7$  TeV. For our phenomenological analysis, we use the NLO set of the MSTW2008 parton distributions [56], corresponding to  $\alpha_s(m_Z) = 0.12018$ . As electroweak input parameters we have chosen  $m_Z = 91.188$  GeV,  $m_W = 80.419$  GeV, and  $G_F = 1.16639 \times 10^{-5}$  GeV<sup>-2</sup>. The other

parameters,  $\alpha_{\text{QED}}$  and  $\sin^2 \theta_W$  are computed thereof via LO electroweak relations. The widths of the weak bosons are set to  $\Gamma_W = 2.099$  GeV and  $\Gamma_Z = 2.51$  GeV. For the reconstruction of jets from final-state partons, we use the **FASTJET** implementation [57] of the  $k_T$  algorithm [58, 59], with a resolution parameter of  $R = 0.4$ .

It is known that using as a scale just the mass of the weak boson gives rise to larger, and shape dependent  $K$ -factors. In Ref. [10] local scales were used that can not be implemented in a straightforward way in the **POWHEG BOX**. This is because the **POWHEG BOX** currently intrinsically assumes that the renormalization scales are the same at all vertices. We therefore set the factorization and renormalization scales here to

$$\mu_R = \mu_F = \frac{p_{T,p1} + p_{T,p2} + E_{T,W_1} + E_{T,W_2}}{2}, \quad \text{with} \quad E_{T,W} = \sqrt{M_W^2 + p_{T,W}^2}, \quad (3.1)$$

where the  $p_{T,pi}$  are the transverse momenta of the two final-state partons of the underlying Born configuration and each  $p_{T,W_i}$  represents the transverse momentum of a same-type lepton-neutrino pair. In the public code, the user is free to implement different scales and use any set of parton distributions (PDFs) available from the LHAPDF library [60]. Process-specific selection cuts can easily be modified in the analysis routine.

As explained in some detail in Ref. [25], in the **POWHEG** method the hardest emission is always generated first, with a technique that yields positive-weighted events using the exact NLO-QCD matrix elements. The **POWHEG** output can thus be interfaced most easily to a parton-shower Monte-Carlo program that is  $p_T$  ordered, or allows the implementation of a  $p_T$  veto. **PYTHIA 6** does adopt transverse-momentum ordering and thus can be interfaced in a straightforward manner to **POWHEG**. On the other hand, angular-ordered parton-shower Monte Carlos, such as **HERWIG**, may generate soft radiation before generating the radiation of highest  $p_T$ . To account for this type of radiation, a vetoed-truncated shower must be included for a fully consistent matching with **POWHEG**. For our phenomenological analysis, we use **PYTHIA 6.4.21** [22] to shower the events, include hadronization corrections and underlying event with the Perugia 0 tune. In this study, QED radiation effects are not taken into account. We have also showered events using **HERWIG 6.51** [21], supplemented by **JIMMY 4.31** for the simulation of multiple parton interactions. While **HERWIG**, utilizing an angular-order parton shower, does not provide the truncated shower required for a fully consistent matching with **POWHEG** at double-logarithmic accuracy, the effect of neglecting the associated contributions is expected to be small [24]. Indeed, we found that for most observables the results obtained by interfacing **POWHEG** to **HERWIG+JIMMY** are very similar to the **POWHEG+PYTHIA** predictions. In the following we will thus focus on **PYTHIA** results.

We require the presence of two jets with transverse momentum larger than  $p_{T,j} = 20$  GeV. The two jets of highest transverse momentum are referred to as “tagging jets”. We note, however, that the cross-section is finite even without any cut on the jets, and that since typical transverse momenta in the event are much larger than 20 GeV (see Fig. 4) the full cross-section without any cut is very close to the numbers quoted in the following. For the scale choice in Eq. (3.1), we obtain an NLO cross-section<sup>1</sup> of 2.12(2) fb for the

---

<sup>1</sup>Here and in the following, our errors are only statistical and do not include theoretical uncertainties such as scale or PDF dependencies of the results.



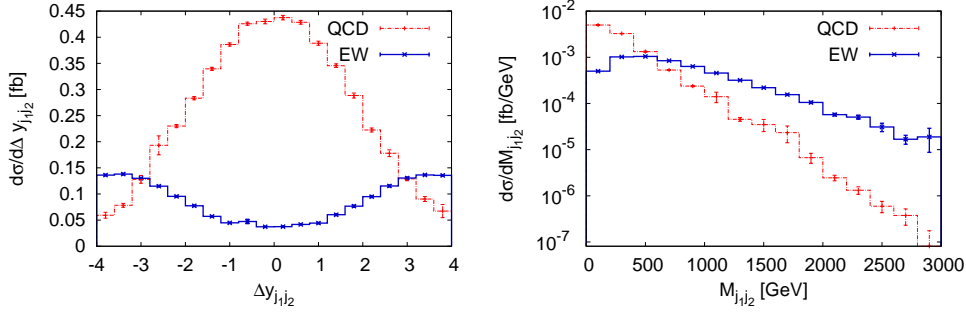


**Figure 3:** Rapidity separation (left panel) and invariant mass (right panel) distributions of the two jets of highest transverse momentum at NLO-QCD accuracy for the QCD (dashed red lines) and EW (solid blue lines) production modes to  $e^+\nu_e\mu^+\nu_\mu jj$  production at the LHC with  $\sqrt{s} = 7$  TeV.

QCD and 1.097(6) fb for the electroweak production mode. For our set-up ( $pp$  collisions at 7 TeV) the QCD cross-section is thus approximately twice as large as the electroweak one. Therefore, as observed already in Ref. [47], despite the hierarchy between the strong and the electroweak coupling constant, the QCD production cross-section is only moderately larger than the electroweak one.

Furthermore, selection cuts that exploit characteristic differences between the two production modes can serve as a powerful tool for the suppression of QCD-induced  $W^+W^+jj$  production, while they reduce the electroweak production cross section only marginally. Imposing such cuts is particularly important in the context of searches for new physics which manifests itself in the weak-boson scattering mode. In order to identify such signatures, an efficient suppression of the QCD background is mandatory.

Figure 3 illustrates the most striking differences between the QCD and electroweak production modes. Jets produced via QCD interactions tend to be close in rapidity. Consequently, the distribution for the rapidity separation of the two tagging jets,  $\Delta y_{j1j2} = y_{j1} - y_{j2}$ , peaks at zero for the QCD  $W^+W^+jj$  production mode. On the other hand, VBF  $W^+W^+jj$  production gives rise to two hard jets in the forward and backward regions of the detector, which are well separated in rapidity. Requiring a large rapidity separation of the two leading jets is thus an efficient tool for enhancing VBF with respect to QCD contributions. Similar differences can be observed for the invariant mass distribution,  $d\sigma/dM_{j1j2}$ , of the two leading jets. Jet pairs of small invariant mass are characteristic for the QCD production mode, while a rather hard invariant mass distribution results from VBF  $W^+W^+jj$  production. Imposing a large invariant-mass cut on the two leading jets thus further reduces the relative impact of QCD contributions on the  $W^+W^+jj$  final state.

In the following we focus on a set of cuts which are specifically designed to enhance electroweak with respect to QCD contributions, making use of the aforementioned features of the two distinct production modes. Since these selection criteria are particularly useful in the phase space region where weak boson scattering is searched for, they are usually referred to as “VBF cuts”. Throughout our phenomenological analysis, we consider jets as

identified only if their transverse momenta are larger than

$$p_{T,j} \geq 20 \text{ GeV} , \quad (3.2)$$

in the rapidity-region accessible to the detector,

$$y_j \leq 4.5 . \quad (3.3)$$

Events with less than two jets fulfilling the criteria of Eqs. (3.2) and (3.3) are disregarded. The two tagging jets are required to be well-separated in rapidity,

$$|\Delta y_{j_1 j_2}| = |y_{j_1} - y_{j_2}| > 4 , \quad (3.4)$$

in opposite hemispheres of the detector,

$$y_{j_1} \times y_{j_2} < 0 , \quad (3.5)$$

with large invariant mass,

$$M_{j_1 j_2} > 600 \text{ GeV} . \quad (3.6)$$

On the two hard charged leptons, we impose the transverse-momentum cut

$$p_{T,\ell} \geq 20 \text{ GeV} , \quad (3.7)$$

and demand that they be located in the central-rapidity region,

$$|y_\ell| \leq 2.5 . \quad (3.8)$$

We furthermore require that they be well-separated from the tagging jets and from each other in the rapidity-azimuthal angle plane,

$$\Delta R_{j\ell} \geq 0.4 , \quad \Delta R_{\ell\ell} \geq 0.1 . \quad (3.9)$$

In addition, the charged leptons are supposed to fall between the two tagging jets in rapidity,

$$\min\{y_{j_1}, y_{j_2}\} < y_\ell < \max\{y_{j_1}, y_{j_2}\} . \quad (3.10)$$

With the above settings, we obtain an NLO-QCD cross section for the VBF production mode of  $\sigma^{\text{cuts}} = 0.201(3) \text{ fb}$ . Therefore cuts reduced the electroweak cross-section by a factor 5. In contrast, the NLO cross-section for the QCD production mode amounts now to only  $0.0074(7) \text{ fb}$ , i.e. the cuts effectively reduced this cross-section by a factor of almost 300. We conclude that once VBF cuts are imposed, the QCD production mechanism becomes insignificant, and we neglect it in the following. After merging the VBF NLO matrix elements with `PYTHIA`, the cross section within the same cuts amounts to  $0.1808(6) \text{ fb}$ . Clearly, due to the extra hadronic activity generated by the shower, fewer events pass the selection criteria that we impose. This change in the cross section should be kept in mind when very precise theoretical predictions are required, as is the case, for instance, in the context of coupling measurements in VBF processes at the LHC [61].

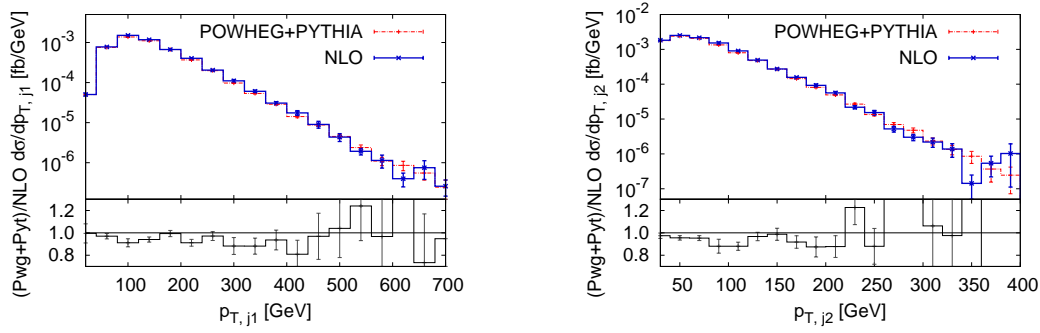


**Figure 4:** Transverse momentum distributions of the two tagging jets at NLO-QCD (solid blue lines) and with POWHEG+PYTHIA (dashed red lines) for  $e^+\nu_e\mu^+\nu_\mu jj$  production at the LHC with  $\sqrt{s} = 7$  TeV. The lower panels show the respective ratios of the POWHEG+PYTHIA to the NLO results.

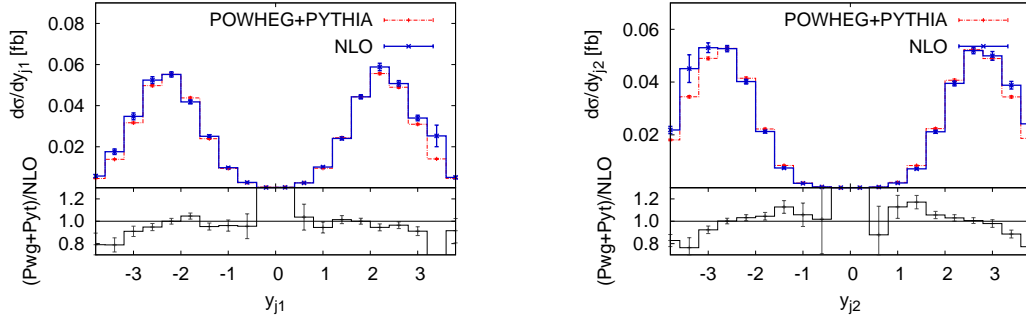


**Figure 5:** Same as Fig. 4 for the rapidity distribution of the hardest tagging jet (left) and second hardest tagging jet (right).

Even though the cross sections differ by around 10%, the shape of the transverse momentum distributions of the two tagging jets, displayed in Fig. 4, are hardly affected by parton shower effects. The production of tagging jets of high rapidity becomes somewhat less likely in the POWHEG+PYTHIA case, however, as illustrated by the rapidity distributions of the two tagging jets in Fig. 5.

Good agreement between NLO and POWHEG+PYTHIA is found for observables related to the two hard charged leptons, such as their transverse momentum and rapidity distributions, which are displayed in Fig. 6 for the positron. Since we neglect lepton-mass effects in the NLO calculation, the corresponding results for the  $\mu^+$  are identical at NLO. While the shapes of these distributions barely change, their magnitudes are reduced in the same way as  $\sigma^{\text{cuts}}$  when the NLO calculation is merged with PYTHIA. This effect can also be observed in the invariant mass distribution of the  $e^+$  and the  $\mu^+$  and in the azimuthal angle separation of the two tagging jets, shown in Fig. 7.

At NLO-QCD, a third jet can only be generated by real-radiation contributions. All observables related to the third jet are therefore effectively known at leading order only. Furthermore, when the NLO matrix element is matched with a parton-shower program, even if the hardest emission is always generated by POWHEG, a third jet can also emerge from the parton shower. It is therefore interesting to compare the fixed-order parton-level pre-

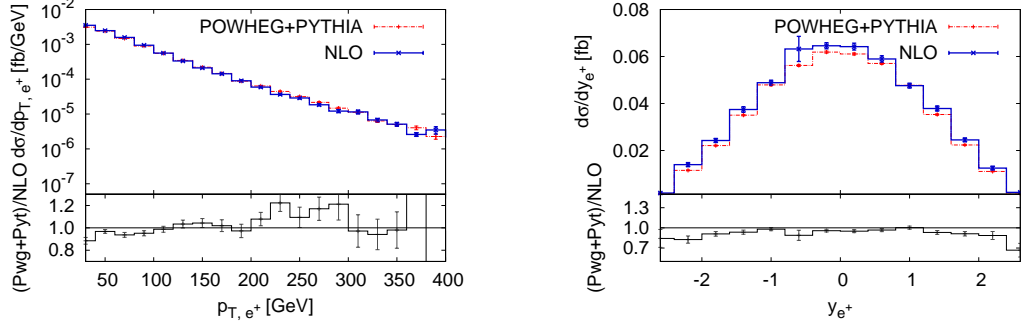


**Figure 6:** Same as Fig. 4 for the transverse momentum (left) and rapidity (right) distributions of the positron.

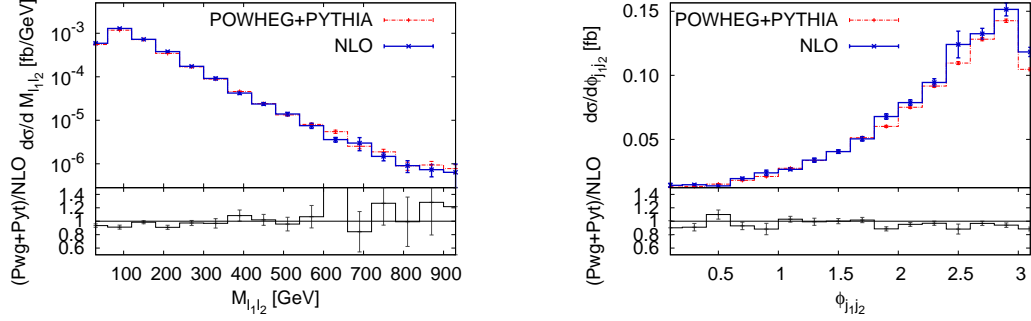


**Figure 7:** Same as Fig. 4 for the invariant mass distribution of the two charged leptons (left) and the azimuthal angle separation of the two tagging jets (right).

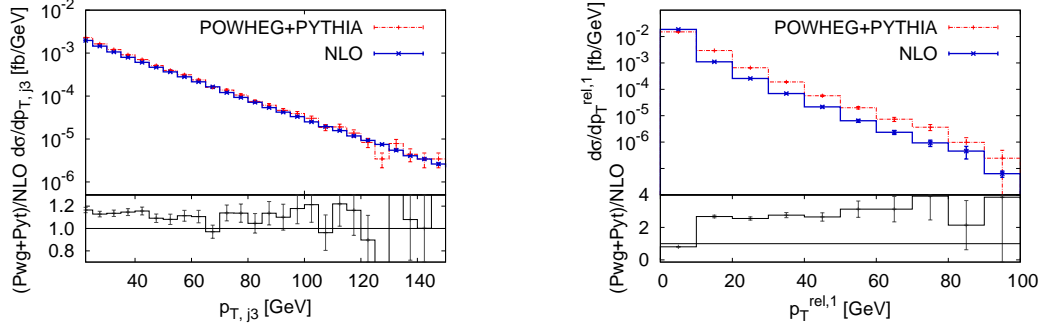


**Figure 8:** Same as Fig. 4 for the transverse momentum distribution of the third jet (left) and relative transverse momentum distribution inside the hardest tagging jet (right).

diction with the POWHEG+PYTHIA result for observables being particularly sensitive to this extra emission. Figure 8 (left panel) shows that for the third jet transverse momentum distributions of very similar shape are obtained with the parton-level and the POWHEG+PYTHIA programs.

The relative distribution of the transverse momenta of all particles inside a jet, defined with respect to the jet axis in the frame where the jet has zero rapidity and momentum

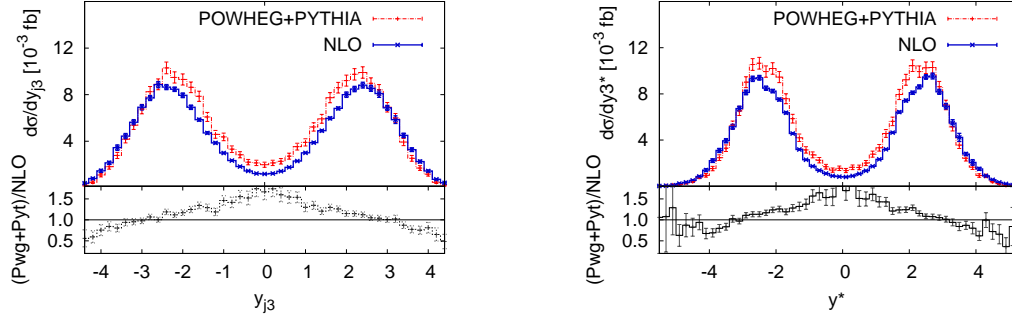


**Figure 9:** Same as Fig. 4 for the rapidity distribution of the third jet (left) and rapidity of the same jet with respect to the average of the rapidities of the two tagging jets,  $y^*$ .

$p_j$ , is given by

$$p_T^{\text{rel},j} = \sum_{i \in j} \frac{|\vec{k}_i \times \vec{p}_j|}{|\vec{p}_j|}. \quad (3.11)$$

Here,  $k_i$  denotes the momentum of the  $i^{\text{th}}$  particle (track) inside the jet. Figure 8 (right panel) illustrates  $p_T^{\text{rel},j}$  for the hardest tagging jet. At LO, only one parton contributes to this jet. The jet axis is thus identical with the associated parton track and  $p_T^{\text{rel},1}$  vanishes. At NLO, real-emission configurations give rise to non-zero values of  $p_T^{\text{rel},1}$ . The largest contribution comes from partons which are quasi-soft or collinear to the hard parton associated with the jet, which results in a divergence of  $d\sigma/dp_T^{\text{rel},1}$  at  $p_T^{\text{rel},1} = 0$ . The POWHEG+PYTHIA prediction is damped in this region, but lies above the pure NLO result everywhere else.

As already mentioned previously, contrary to QCD-mediated reactions, in weak boson scattering processes jet activity in the central-rapidity region is suppressed due to the color-singlet nature of the weak boson exchange in the  $t$ -channel. This feature can be exploited for background suppression by imposing a central jet veto, i.e., discarding all events which exhibit substantial jet activity in the rapidity region between the two tagging jets [62]. For employing central-jet veto techniques reliably in realistic simulations it is crucial to quantitatively understand the impact of parton-shower effects on jet emission in the central-rapidity range. In the context of Higgs production via VBF, to this end detailed studies have been performed [37, 63–65]. Similarly to what happens in Higgs production via VBF, in  $pp \rightarrow W^+W^+jj$  differences between the parton-level and the POWHEG+PYTHIA results occur in the rapidity distribution of the third jet. As illustrated by Fig. 9 (left panel), in the pure NLO case a distinct dip occurs in  $d\sigma/dy_{j_3}$ , which is partially washed out in the POWHEG+PYTHIA result, thus weakening the case of a central jet veto.

The position of the third jet with respect to the average of the two tagging jets can be accessed by the observable  $y^*$ , which is defined as

$$y^* = y_{j_3} - \frac{y_{j_1} + y_{j_2}}{2} \quad (3.12)$$

and is displayed in Fig. 9 (right panel). When the third jet is located in the central-rapidity region,  $y^*$  is close to zero, while  $|y^*|$  values of about three indicate that the third jet is

close to one of the tagging jets, as is obvious from the position of the peaks in the rapidity distributions of the two tagging jets (c.f. Fig. 5). If a parton ends up close to one of the tagging jets, it is likely to be recombined into this hard jet rather than giving rise to an extra jet [65]. From Fig. 9 it becomes apparent that the extra hadronic activity due to the parton shower when POWHEG is matched with PYTHIA is preferentially emitted in the region between the two tagging jets.

## 4. Conclusion

In this work, we presented the implementation of the NLO-QCD calculation for electroweak  $W^+W^+jj$  production in hadronic collisions in the POWHEG BOX [34], a framework which allows the merging of NLO-QCD calculations with parton-shower programs such as PYTHIA and HERWIG. In this way the accurate perturbative description of the hard partonic scattering event can be combined in a well-defined manner with a realistic simulation of the hadronic environment in  $pp$  collisions. Our implementation is publicly available following the instructions provided at the POWHEG BOX web site <http://powhegbox.mib.infn.it>.

With its distinct signature, the reaction  $pp \rightarrow W^+W^+jj$  is interesting not only from a technical point of view, but also as a background for new physics searches and double parton scattering processes. It receives contributions from QCD and EW production modes. The QCD  $W^+W^+jj$  production has already been considered in the framework of the POWHEG BOX in Ref. [45]. Our new implementation of the EW production mode in the POWHEG BOX allowed us to perform a phenomenological comparison of the two processes, going beyond the estimates of Ref. [14]. While naively one could expect the QCD contributions to be much larger than the EW ones, the QCD cross section is only approximately twice as large as the EW one for inclusive cuts. VBF-specific selection cuts further suppress the QCD contributions efficiently, resulting in a ratio  $\sigma_{\text{QCD}}^{\text{cuts}}/\sigma_{\text{EW}}^{\text{cuts}} \approx 0.04$ . We conclude that in the range where weak boson scattering is searched for experimentally, no significant contamination from QCD-induced  $W^+W^+jj$  production is to be expected.

In this region, we have studied the impact of parton-shower effects on NLO-QCD results for several characteristic distributions. We found only a mild distortion of selected observables, such as rapidity distributions of the hardest jets and leptons. Larger differences between the NLO parton-level and the POWHEG+PS predictions can be encountered, however, for the rapidity of the third jet. A quantitative understanding of observables related to the third jet is important if central-jet vetoing techniques are to be utilized at the LHC.

**Acknowledgments** We are grateful to Paolo Nason for helpful comments regarding the implementation in the POWHEG BOX. We thank Carlo Oleari and Dieter Zeppenfeld for a careful proof-reading of the manuscript and for their valuable feedback. We furthermore would like to thank Gavin Salam and Simon Plätzer for useful discussions. The work of B. J. is supported by the Research Center *Elementary Forces and Mathematical Foundations (EMG)* of the Johannes-Gutenberg-Universität Mainz. G. Z. is supported by the British Science and Technology Facilities Council, by the LHCPHenoNet network under the Grant Agreement PITN-GA-2010-264564 and by the European Research and Training Network (RTN) grant Unification in the LHC ERA under the Agreement PITN-GA-2009-237920.

## References

- [1] R. K. Ellis, Z. Kunszt, K. Melnikov, G. Zanderighi, arXiv:1105.4319 [hep-ph].
- [2] A. Bredenstein, A. Denner, S. Dittmaier, S. Pozzorini, JHEP **1003** (2010) 021. [arXiv:1001.4006 [hep-ph]].
- [3] G. Bevilacqua, M. Czakon, C. G. Papadopoulos, R. Pittau, M. Worek, JHEP **0909** (2009) 109. [arXiv:0907.4723 [hep-ph]].
- [4] C. F. Berger *et al.*, Phys. Rev. **D80** (2009) 074036. [arXiv:0907.1984 [hep-ph]].
- [5] R. K. Ellis, K. Melnikov, G. Zanderighi, JHEP **0904** (2009) 077. [arXiv:0901.4101 [hep-ph]].
- [6] R. K. Ellis, K. Melnikov, G. Zanderighi, Phys. Rev. **D80** (2009) 094002. [arXiv:0906.1445 [hep-ph]].
- [7] T. Binoth, N. Greiner, A. Guffanti, J. Reuter, J. -P. Guillet, T. Reiter, Phys. Lett. **B685** (2010) 293-296. [arXiv:0910.4379 [hep-ph]].
- [8] G. Bevilacqua, M. Czakon, C. G. Papadopoulos, M. Worek, Phys. Rev. Lett. **104** (2010) 162002. [arXiv:1002.4009 [hep-ph]].
- [9] C. F. Berger *et al.*, Phys. Rev. **D82** (2010) 074002. [arXiv:1004.1659 [hep-ph]].
- [10] B. Jäger, C. Oleari, D. Zeppenfeld, Phys. Rev. **D80** (2009) 034022. [arXiv:0907.0580 [hep-ph]].
- [11] G. Bozzi, B. Jäger, C. Oleari, D. Zeppenfeld, Phys. Rev. **D75** (2007) 073004. [arXiv:hep-ph/0701105].
- [12] B. Jäger, C. Oleari, D. Zeppenfeld, Phys. Rev. **D73** (2006) 113006. [arXiv:hep-ph/0604200].
- [13] B. Jäger, C. Oleari, D. Zeppenfeld, JHEP **07** (2006) 015. [arXiv:hep-ph/0603177].
- [14] T. Melia, K. Melnikov, R. Rontsch, G. Zanderighi, JHEP **1012** (2010) 053. [arXiv:1007.5313 [hep-ph]].
- [15] S. Dittmaier, P. Uwer, S. Weinzierl, Phys. Rev. Lett. **98** (2007) 262002. [arXiv:hep-ph/0703120].
- [16] A. Denner, S. Dittmaier, S. Kallweit, S. Pozzorini, Phys. Rev. Lett. **106** (2011) 052001. [arXiv:1012.3975 [hep-ph]].
- [17] G. Bevilacqua, M. Czakon, A. van Hameren, C. G. Papadopoulos, M. Worek, JHEP **02** (2011) 083. [arXiv:1012.4230 [hep-ph]].
- [18] C. F. Berger *et al.*, [arXiv:1009.2338 [hep-ph]].
- [19] F. Campanario, C. Englert, M. Rauch, D. Zeppenfeld, arXiv:1106.4009 [hep-ph].
- [20] G. Marchesini *et al.*, Comp. Phys. Commun. **67** (1992) 465.
- [21] G. Corcella *et al.*, JHEP **0101** (2001) 010. [hep-ph/0011363].
- [22] T. Sjostrand, S. Mrenna, P. Z. Skands, JHEP **0605** (2006) 026. [hep-ph/0603175].
- [23] S. Frixione, B. R. Webber, JHEP **0206** (2002) 029. [hep-ph/0204244].
- [24] P. Nason, JHEP **0411** (2004) 040. [hep-ph/0409146].
- [25] S. Frixione, P. Nason, C. Oleari, JHEP **0711** (2007) 070. [arXiv:0709.2092 [hep-ph]].

- [26] V. Hirschi *et al.*, JHEP **1105** (2011) 044 [arXiv:1103.0621 [hep-ph]].
- [27] R. Frederix *et al.*, arXiv:1104.5613 [hep-ph].
- [28] M. Bahr *et al.*, Eur. Phys. J. C **58** (2008) 639. [arXiv:0803.0883 [hep-ph]].
- [29] L. D’Errico, P. Richardson, arXiv:1106.3939 [hep-ph]; arXiv:1106.2983 [hep-ph].
- [30] T. Gleisberg *et al.*, JHEP **02** (2009) 007. [arXiv:0811.4622].
- [31] S. Hoche, F. Krauss, M. Schonherr, F. Siegert, JHEP **04** (2011) 024. [arXiv:1008.5399 [hep-ph]].
- [32] A. Kardos, C. Papadopoulos and Z. Trocsanyi, arXiv:1101.2672 [hep-ph].
- [33] M. V. Garzelli, A. Kardos, C. G. Papadopoulos and Z. Trocsanyi, arXiv:1108.0387 [hep-ph].
- [34] S. Alioli, P. Nason, C. Oleari, E. Re, JHEP **1006** (2010) 043. [arXiv:1002.2581 [hep-ph]].
- [35] S. Frixione, P. Nason, G. Ridolfi, JHEP **09** (2007) 126. [arXiv:0707.3088 [hep-ph]].
- [36] S. Alioli, P. Nason, C. Oleari, E. Re, JHEP **04** (2009) 002. [arXiv:0812.0578 [hep-ph]].
- [37] P. Nason, C. Oleari, JHEP **1002** (2010) 037. [arXiv:0911.5299 [hep-ph]].
- [38] S. Alioli, P. Nason, C. Oleari, E. Re, JHEP **07** (2008) 060. [arXiv:0805.4802 [hep-ph]].
- [39] S. Alioli, P. Nason, C. Oleari, E. Re, JHEP **1101** (2011) 095. [arXiv:1009.5594 [hep-ph]].
- [40] S. Alioli, P. Nason, C. Oleari, E. Re, JHEP **09** (2009) 111. [arXiv:0907.4076 [hep-ph]].
- [41] E. Re, Eur. Phys. J. **C71** (2011) 1547. [arXiv:1009.2450 [hep-ph]].
- [42] S. Alioli, K. Hamilton, P. Nason, C. Oleari, E. Re, JHEP **04** (2011) 081. [arXiv:1012.3380 [hep-ph]].
- [43] C. Oleari, L. Reina, arXiv:1105.4488 [hep-ph].
- [44] T. Melia, P. Nason, R. Rontsch, G. Zanderighi, arXiv:1107.5051 [hep-ph].
- [45] T. Melia, P. Nason, P. Rontsch, G. Zanderighi, arXiv:1102.4846 [hep-ph].
- [46] A. Kulesza, W. J. Stirling, Phys. Lett. **B475** (2000) 168-175. [hep-ph/9912232];  
E. Maina, JHEP **0909** (2009) 081. [arXiv:0909.1586 [hep-ph]].
- [47] J. R. Gaunt, C. H. Kom, A. Kulesza, W. J. Stirling, Eur. Phys. J. C **69** (2010) 53 [arXiv:1003.3953 [hep-ph]].
- [48] H. K. Dreiner, S. Grab, M. Kramer, M. K. Trenkel, Phys. Rev. **D75** (2007) 035003. [hep-ph/0611195].
- [49] J. Maalampi, N. Romanenko, Phys. Lett. **B532** (2002) 202. [hep-ph/0201196].
- [50] K. Arnold *et al.*, Comp. Phys. Comm. **180** (2009) 1661. [arXiv:0811.4559 [hep-ph]];  
K. Arnold *et al.*, arXiv:1107.4038 [hep-ph].
- [51] M. Ciccolini, A. Denner, S. Dittmaier, Phys. Rev. **D77** (2008) 013002. [arXiv:0710.4749 [hep-ph]].
- [52] A. Denner, S. Dittmaier, Nucl. Phys. **B658** (2003) 175. [hep-ph/0212259].
- [53] A. Denner, S. Dittmaier, Nucl. Phys. **B734** (2006) 62. [hep-ph/0509141].
- [54] S. Catani, M. H. Seymour, Nucl. Phys. **B485** (1997) 291. [hep-ph/9605323].



- [55] S. Frixione, Z. Kunszt, A. Signer, Nucl. Phys. **B467** (1996) 399. [hep-ph/9512328].
- [56] A. D. Martin, W. J. Stirling, R. S. Thorne, G. Watt, Eur. Phys. J. **C63** (2009) 189-285. [arXiv:0901.0002 [hep-ph]].
- [57] M. Cacciari, G. P. Salam, Phys. Lett. **B641** (2006) 57. [hep-ph/0512210].
- [58] S. Catani, Y. L. Dokshitzer, M. H. Seymour, B. R. Webber, Nucl. Phys. **B406** (1993) 187.
- [59] S. D. Ellis, D. E. Soper, Phys. Rev. **D48** (1993) 3160. [hep-ph/9305266].
- [60] M. R. Whalley, D. Bourilkov, R. C. Group, hep-ph/0508110.
- [61] M. Duhrssen *et al.* Phys. Rev. **D70** (2004) 113009. [hep-ph/0406323].
- [62] D. L. Rainwater, R. Szalapski, D. Zeppenfeld, Phys. Rev. **D54** (1996) 6680. [hep-ph/9605444].
- [63] T. Figy, C. Oleari, D. Zeppenfeld, Phys. Rev. **D68** (2003) 07300. [hep-ph/0306109].
- [64] T. Figy, V. Hankele, D. Zeppenfeld, JHEP **02** (2008) 076. [arXiv:0710.5621[hep-ph]].
- [65] C. Hackstein, Diploma thesis, Karlsruhe University,  
<http://www-itp.particle.uni-karlsruhe.de/diplomatheses.de.shtml>